EVALUATION OF A LOW-COST PHOTOGRAMMETRIC SYSTEM FOR THE RETRIEVAL OF 3D TREE ARCHITECTURE

A. Zaforemska[1]*, R. Gaulton[2], J. Mills[1], W. Xiao[3]

[1] School of Engineering, Newcastle University, UK - (a.zaforemska2, jon.mills)@newcastle.ac.uk
[2] School of Natural and Environmental Sciences, Newcastle University, UK - rachel.gaulton@newcastle.ac.uk
[3] School of Geography and Information Engineering, China University of Geosciences, China - wen.xiao@cug.edu.cn

Commission II, WG II/1

KEY WORDS: Photogrammetry, Structure-from-Motion, TLS, Low-cost camera, Tree architecture

ABSTRACT:

Reconstruction of major branches of a tree is an important first step for the monitoring of tree sway and assessment of structural stability. Photogrammetric systems can provide a low-cost alternative for the acquisition of three-dimensional data, while also enabling long-term monitoring of a tree of interest. This study introduces a low-cost photogrammetric system based on two Raspberry Pi cameras, which is used to reconstruct the tree architecture for the purpose of stability monitoring. Images of five trees are taken at a range of distances and the resulting point clouds are evaluated in terms of point density and distribution with the reference to TLS. While the photogrammetric point clouds are sparse, it was found that they are capable of reconstructing the tree trunk and lower-order branches, which are most relevant for sway monitoring and tree stability assessment. The most optimal distance for the reconstruction of the relevant branches was found to be 9-10 m, with a baseline of 120 cm.

1. INTRODUCTION

Urban trees are a crucial element of green infrastructure, providing a range of valuable ecosystem services. They contribute to the reduction of pollution (Willis and Petrokofsky, 2017) and temperature regulation (Doick et al., 2014) in the cities, providing shade and potentially reducing energy use. Their presence in urban areas has also been linked to improvements in mental and physical well-being, since they may encourage physical activity outdoors. This also links to some of the indirect social and economic benefits, as well-maintained trees contribute to the increase in value of a neighbourhood, reduction of crime and can potentially encourage more visitors to use the local shops and amenities (Turner-Skoff and Cavender, 2019). As a result, campaigns promoting increased tree planting in cities have gained popularity (Sousa-Silva et al., 2023). While such initiatives have many benefits, they can also incur significant costs associated with care and maintenance. Climate change causes more frequent and intense extreme weather events, potentially leading to declining tree health. Long periods of drought weaken the trees and make them more vulnerable to breakage, while intense rainfalls cause high soil saturation and increase the risk of uprooting. Urban trees are particularly vulnerable to branch failures and structural defects, increasing the risk of damage in high wind (Nelson et al., 2022). A study by (van Haaften et al., 2016) conducted in the Netherlands has found that tree failure events are occurring three times as often now as fifty years ago and the upward trend continues. These events have significant implications for public safety, as tree failure leads not only to damage to property and infrastructure but also loss of health and life. Regular monitoring and maintenance are therefore essential to ensure the trees' healthy condition and reduce the risk of failure. In practice, manual tree surveys in urban areas are often performed infrequently and the maintenance is primarily reactive. While it is still vital to consider the existing damage to the trees and their health while conducting the risk assessments, more data is required to fully understand the tree response to wind. For this reason, a number of studies have been conducted which looked at the monitoring of wind-induced tree sway using strain gauges, accelerometers and inclinometers (Jackson et al., 2020). However, the main limitation of these methods is that they take measurements only at a specific point on a tree, usually the tree trunk, often omitting branches. While the failure of the tree as a whole has the potential to cause the most damage, it happens less frequently than branch failure, which can also be harmful. For this reason, it is important to develop a method which would enable the monitoring of the frequency and degree of movement of not only the tree trunk but also the branches and the crown as a whole. 3D data capture methods like laser scanning enable fast acquisition of detailed models of tree architecture, which could be valuable for the assessment of the tree's overall structural condition. Still, the high costs might limit their widespread adoption. Furthermore, laser scanning may not be suitable for the monitoring of tree sway, due to the time needed for data capture - it is not possible to record high-frequency movements. Close-ranged terrestrial photogrammetry has the potential to provide a more accessible alternative, with single-board cameras serving as a basis for low-cost photogrammetric and monitoring systems. While previous studies using similar devices focused on building models from multiple viewpoints (Miller et al., 2015)(Mokroš et al., 2017), our approach looks at the simple scenario of two cameras installed on a single rail with a modifiable baseline, which allows us to achieve optimal depth accuracy. This system is suitable for long-term deployment for the purpose of monitoring the wind-induced sway and structural condition of high-value and high-risk trees.

2. AIMS AND OBJECTIVES

In order to use the photogrammetric system for tracking the sway of a tree and its branches in three dimensions, first it has to be determined how well the features can be detected and reconstructed. This work serves as an initial part of a broader

study and its scope is limited to the evaluation of 3D reconstruction quality in terms of its utility for tree sway monitoring. This is achieved by comparing the point clouds obtained with the photogrammetric method with point clouds from terrestrial laser scanning, which will serve as a benchmark. We are also considering the depth resolution and field of view, by testing the photogrammetric system at a range of distances from the target tree. It is important to highlight that as the goal is to be able to track the tree elements with the highest potential for failure and damage, it is not essential to obtain a very dense and complete point cloud. Some of the highest-order branches are very difficult to reconstruct due to how fine and densely growing they can be. However, these are also the branches that have a very low impact upon failure. For this reason, the study assesses the completeness and accuracy of the point cloud at each branching order of the tree, with higher importance given to the lower orders.

3. METHODOLOGY

3.1 Equipment

The camera system developed for this study is based on two Raspberry Pi Zero W computing boards coupled with Raspberry Pi v2 NoIR cameras. The main benefit of this setup is its cost - approximately £10 per board and £24 per camera. Despite the low price point, the cameras can achieve relatively good image quality with resolutions up to 3,280 x 2,464 pixels and can be easily programmed to capture imagery at a range of parameters. The further specifications of the camera model can be seen in Table 1. The additional advantage of the NoIR camera is the lack of an infrared blocking filter, which allows for data acquisition in low-light environments and the capture of IR information, especially beneficial for vegetation monitoring applications. Additionally, the Zero boards, in comparison to full-size Raspberry Pi 4, benefit from portability and lower power usage, which is particularly important for the potential long-term deployment of the system. Both boards are connected to a single button which triggers the image capture, ensuring that both of the cameras are synchronised to 0.02 seconds. This is essential for data collection in windy conditions, as branches have to be in the exact same positions in both of the images for successful reconstruction. The cameras are positioned in parallel on a rail, which provides a modifiable baseline (Figure 1).

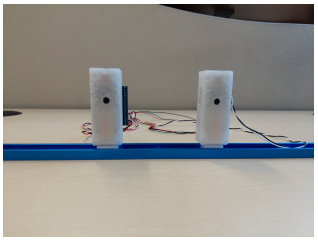

Figure 1. The camera system used in the experiment.

Sensor	Sony IMX219
Focal length	3.04 mm
Field of view (horizontal)	62.2 deg
Field of view (vertical)	48.8 deg
Resolution	3280x2464 px
Sensor area	3.68 x 2.76 mm
Pixel size	1.12 µm x 1.12 µm

Table 1. Raspberry Pi v2 camera specification.

Both of the cameras were geometrically calibrated with Agisoft Metashape Lens Calibration module (Agisoft, 2023). This method uses a fixed chessboard pattern, which is then photographed from a range of angles and distances. The calibration parameters are then applied to each image obtained from the corresponding camera. To obtain the reference point cloud, we used Leica RTC360 terrestrial laser scanner. This model of scanner has been previously used for obtaining point clouds of trees both in the forests (Ko et al., 2022), as well as in urban context (Jaalama et al., 2021).

3.2 Experimental setup

The imagery and point cloud data were collected over the period of late April-early May 2023 in Exhibition Park, Newcastle upon Tyne, United Kingdom. Four species of trees were selected for the study: two common ash (A1 and A2) (*Fraxinus excelsior*), one Swedish whitebeam (W1)(*Sorbus intermedia*), common lime (L1) (*Tilia* × *europaea*) and sycamore (S1) (*Acer pseudoplatanus*). The trees were selected for their ease of access and exposure, allowing the capture of their crowns with limited occlusion.

Figure 2. Example set up of targets around the trees of interest.

The trees were first scanned with the TLS in a semi-circle, with approximately 5-7 stations per tree. The semi-circle was deemed sufficient, as the photogrammetric system would only be capable of reconstructing the trees from one point of view and the TLS managed to capture all parts of the crown without completely encircling the tree. As the automatic pre-alignment process of Leica RTC360 is prone to errors, black and white reflective targets were set up near the trees. This also allowed for an easy alignment with the photogrammetric point clouds. The baseline between the cameras was set as constant at 120 cm. The wide baseline was mainly selected to ensure the reconstruction at further distances (>10 m) with relatively low error. Such distances are important to consider from the perspective of deployment e.g. to monitor trees across the road. The images were taken at a range of distances (5-12 metres) from the target tree, measured from the tree trunk to the level of the camera lens. The cameras were angled slightly upwards (by around 20 degrees), to ensure that most of the image is occupied by the tree crown instead of the ground.

3.3 Data processing

Stereo reconstruction is the most intuitive solution for 3D reconstruction from an image pair, however, it depends on the very precise stereo calibration of the cameras. The cameras

have to be fixed in the exact same position in relation to each other. This proved to be problematic in the outdoor setting, where any movement of the rig would lead to a slight displacement of the cameras and the stereo reconstruction would fail to produce a point cloud. For this reason, we decided to follow the structure-from-motion approach. The TLS point clouds were pre-processed using Leica Register360 and the photogrammetric point clouds were reconstructed using Agisoft Metashape. The images were first loaded in pairs (one per pair chunk) and aligned with the accuracy set to 'high'. Markers were added to the images corresponding to the same targets visible in TLS, to ensure both point clouds are sharing the same local coordinate system. The cameras were then optimised using the parameters obtained through the initial camera calibration. Finally, dense matching was performed, with quality set to 'ultra high'. In order to check if initial image segmentation has the potential to improve the reconstruction of trees, masks were applied to selected image pairs, allowing for the detection of key points only within the area of the image occupied by the tree.

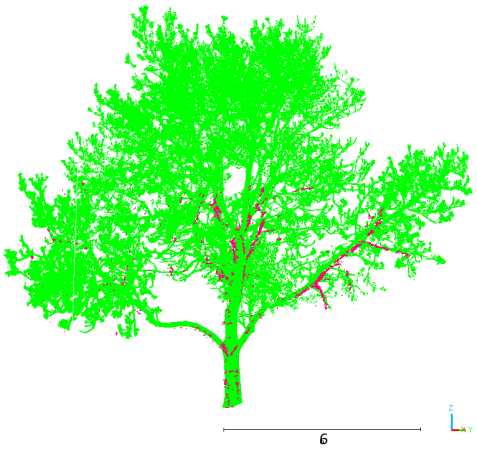

Figure 3. Photogrammetric point cloud (red) plotted against TLS (green) on the example of A1.

The point clouds were then migrated into CloudCompare (CloudCompare, 2020), where they were segmented so that only the points belonging to the tree remained. Photogrammetric point clouds were then finely registered with their corresponding TLS (Figure 3). In order to compare the two point clouds we applied M3C2 (multiscale model-to-model cloud comparison) algorithm available as a plug-in in Cloudcompare. M3C2 was originally developed for detecting a topographic change in point cloud time series (Lague et al., 2013), however, it has also been recently applied in the evaluation of point clouds created using different methods (Cutugno et al., 2022). It uses a cylindrical buffer formed from the selected 'core points' from the reference cloud, to look for the nearest-neighbour points within the corresponding cloud and calculate the distance between them. In this case, we selected the TLS to serve as the core points, with normals diameter set to 0.06 and calculation mode set to 'horizontal'. Photogrammetric point clouds are also examined in terms of point distribution per branch order, which was calculated using from TLS point clouds with the TreeQSM package (Raumonen, 2017).

D	*A1*	*A2*	*L1*	*S1*	*W2*
5	308,051	150,051	206,764	366,245	65,204
6	320,607	210,274	101,037	302,636	60,792
7	402,297	120,043	268,019	339,292	64,719
8	352,447	198,804	231,859	172,499	125,481
9	201,574	216,413	308,886	137,352	144,159
10	278,514	247,158	178,165	636,721	155,740
11	247,536	256,104	NA	143,850	43,778
12	132,352	216,828	NA	96,132	42,473
LS	5,351,813	974,119	3,044,200	3,407,502	9,737,823

Table 2. Number of points per tree at each distance *D* (metres) in photogrammetric and laser scanning *LS* point clouds.

Tree ID	Points (no mask)	Points (mask)
A1	132,352	120,911
A2	216,828	145,369
W1	42,473	49,016
L1	178,165	167,338
S1	96,132	NA

Table 3. Number of points per tree processed without initial image segmentation and masking and after applying the mask.

4. RESULTS

4.1 SfM point cloud generation

As predicted, photogrammetric point clouds generated from the image pairs have significantly lower point density than those obtained with the terrestrial laser scanner (Table 2). A2 has on average the highest proportion of photogrammetric points compared to TLS, at 201,959 points which is approximately 20%. W1 has the highest discrepancy between the TLS and photogrammetric cloud, with 85,793 points on average (0.9%). The values for L1 at 11 and 12 metres are missing from the data table, as the point cloud at those distances could not be resolved. This is likely due to the lack of sufficient features - the tree itself is relatively small (approx. 5 m) and with a narrow crown, so at the larger distances the image is largely occupied by the sky and other background features. This could also be the reason for the lower numbers of points at the distance of 12 metres for the other trees. While there appears to be no strong relationship between the distance from the object and the number of tree points, in most cases the highest values can be observed at 9-10 metres. The trend is most prominent in W1, where the number of points grows from about 7 to 10 metres, to fall again at 11-12 metres. Part of the reason is due to the same issue mentioned above - the presence of background.

Figure 4. Swedish whitebeam *(Sorbus intermedia)* with the built structure (in red circle).

Branch level	5	6	7	8	9	10	11	12	LS
Ash1									
1	92.81	72.87	74.76	50.44	44.52	59.27	70.25	32.77	***8.25***
2	6.61	25.12	22.66	32.16	27.49	24.25	12.56	30.95	***10.43***
3	0.47	1.94	1.03	10.94	11.15	9.5	5.3	12.04	***18.89***
4	0.1	0.07	0.3	4.31	10.6	2.63	5.34	12.92	***28.9***
5	0	0	1.09	1.8	4.05	1.82	5.21	9.21	***21.95***
6	0	0	0	0.05	2.07	2.5	0.95	2.07	***8.59***
7	0	0	0.12	0.31	0.05	0.04	0.38	0.04	***2.53***
8	0	0	0	0	0.06	0	0	0	***0.04***
9	0	0	0	0	0	0	0	0	***0.04***
Ash2									
1	80.54	49.15	46.94	22.3	34.7	18.3	47.74	14.66	***24.24***
2	7.81	5.02	25.36	37.7	16.3	38.8	17.76	26.144	***21.43***
3	8.64	0	25.57	11.4	31.1	9.5	13.39	25.52	***20.94***
4	1.32	20.83	0.58	4.05	7.2	10.96	6.2	19.3	***16.73***
5	1.67	25	1.01	13.09	4.9	12.2	7.99	10.29	***10.18***
6	0	0	0.53	4.06	4	1.04	10.94	0.95	***4.76***
7	0	0	0	7.3	1.7	8.1	1.92	6.12	***1.46***
8	0	0	0	0	0	0	0.04	0	***0.24***
Lime									
1	91.52	93.1	95.79	92.13	92.52	85.93	NA	NA	***11.85***
2	4.41	2.82	1.7	3	3.21	5.81	NA	NA	***11.01***
3	2.83	2.21	1.89	2.85	2.04	4.34	NA	NA	***25.16***
4	1	1.48	0.38	1.39	1.44	2.13	NA	NA	***28.04***
5	0.18	0.29	0.2	0.48	0.65	1.58	NA	NA	***16.33***
6	0.06	0.09	0.04	0.14	0.12	0.17	NA	NA	***6.03***
7	0.002	0.005	0.004	0.005	0.02	0.02	NA	NA	***1.34***
8	0	0	0	0	0.001	0.0006	NA	NA	***0.19***
9	0	0	0	0	0	0	0	0	***0.03***
Sycamore									
1	97.83	92.64	94.78	75.19	86.11	77.52	89.78	85.58	***20.97***
2	1.61	4.47	2.8	10.17	8.42	10.07	7.25	10.3	***29.21***
3	0.55	2.87	2.28	11.48	5.34	8.79	2.58	3.77	***31.16***
4	0.002	0.02	0.14	2.76	0.12	2.62	0.29	0.28	***11.66***
5	0	0	0	0.31	0.006	0.68	0.04	0.06	***4.93***
6	0	0	0	0.07	0	0.29	0.06	0.002	***1.64***
7	0	0	0	0.02	0	0	0	0	***0.35***
8	0	0	0	0	0	0	0	0	***0.06***
9	0	0	0	0	0	0	0	0	***0.004***
Whitebeam									
1	97.84	90.67	39.11	24.24	63.15	40.87	77.19	23.65	***33.5***
2	2.16	6.88	13.33	16.86	19.25	31.5	13.49	13.69	***16.17***
3	0.003	2.44	26.22	30.1	8.3	12.2	6.17	22.22	***14.66***
4	0	0.01	10.67	13.64	3.7	6.48	0.84	13.92	***14.33***
5	0	0	10.67	8.48	3.47	4.54	1.13	14.79	***11.04***
6	0	0	0	5.48	1.62	3.3	0.66	10.89	***7.52***
7	0	0	0	1.18	0.42	1	0.49	0.77	***2.44***
8	0	0	0	0	0.07	0.07	0.01	0.05	***0.25***
9	0	0	0	0	0.007	0	0	0	***0.03***

Table 4. Proportion of points (%) per branching order, at a range of distances and in laser scanning (LS) point clouds.

In the case of these image pairs, there is a small building present next to the target tree. The building is covered in bright graffiti, which provides plenty of high-quality geometric features (Figure 4). These are significantly easier to detect and match than any of the features on the tree (Figure 5). Furthermore, the crown of the whitebeam is very dense, with relatively thin branches, exacerbating the difficulty in finding keypoints within the tree.

4.2 Impact of masking

Due to the impact of the background discussed above, we performed manual segmentation and masking on the images, to determine if it improves the keypoint detection and matching, potentially resulting in denser higher quality point clouds. The test was performed using the images captured at the furthest distance from the target tree where the point clouds resolved - 10 metres for lime and 12 metres for the other species. The resulting point clouds do not differ significantly from the point clouds obtained without the masking and in most cases, the number of tree points is lower. The only exception is W1, where the number of tree points is slightly higher after applying the mask, which may confirm the theory that fewer points found on the tree are due to the feature-rich elements in the background. However, it must be noted that despite masking most of the background, the targets were also included in the matching process and these areas of the image include a high number of keypoints. Further investigation is needed to determine if the quality of the initial segmentation plays a significant role in the improvement of point cloud generation.

4.3 Point distribution

As the final goal of the system is to be able to monitor the sway and stability of the tree and its key branches, rather than looking at the size of the point cloud it is more important to

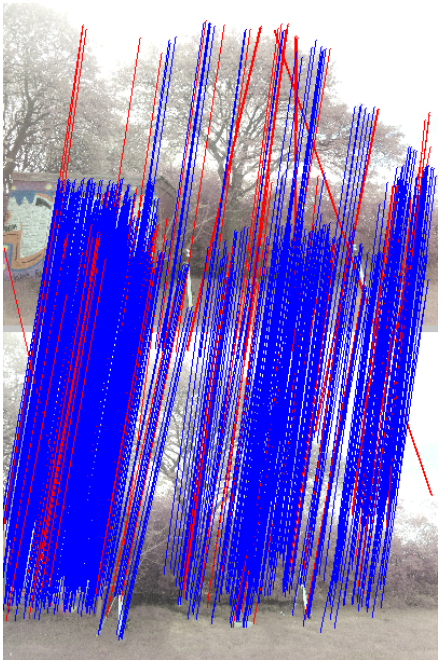

Figure 5. Tie points detected in the whitebeam image pair taken at a distance of 11 metres. Blue lines indicate valid matches and red - invalid.

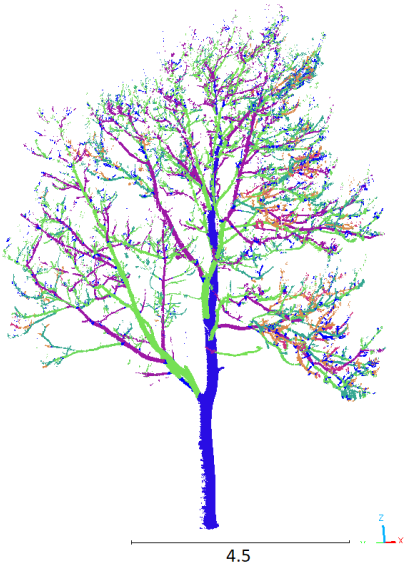

Figure 6. A2 point cloud classified by the branching order.

determine how the points are distributed on the tree. Higher-order branches are usually much smaller in diameter and if they fail, they cause very little to no harm. It is then of paramount importance to reconstruct the lower-order branches at the tree trunk. For this reason, we classified the tree point clouds by the branching order (Figure 6) and examined the proportion of points associated with each level (Table **??**). In the case of our analysis level 1 indicates the tree trunk, while first-order branches (growing directly from the tree trunk) are included in level 2. Due to its high accuracy and coverage, the laser scanning (LS) point cloud can be used to reflect the actual distribution of branches across the tree structure. In most cases, the LS points are relatively evenly distributed across branching levels, with a significantly lower proportion of points only in the highest-order branches, which makes sense due to their smaller size. These branches are almost impossible to resolve within the photogrammetric point clouds, even when the whole tree is present in the field of view of the camera, such as at a distance of 10-12 metres. For A2 and W1, the highest proportion of LS points can be found on the tree trunk, which reflects their structure - a prominent tree trunk with larger less dense branches (ash) or smaller highly dense branches (whitebeam).

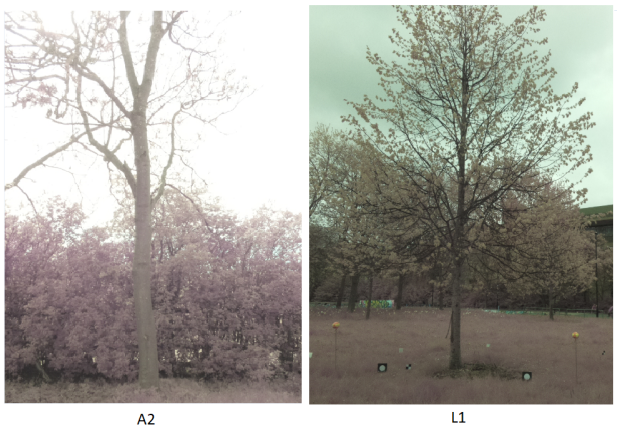

Figure 7. Presence of foliage in the captured trees. Ash (A2) - leaf-off, lime (L1) - partially leaf-on.

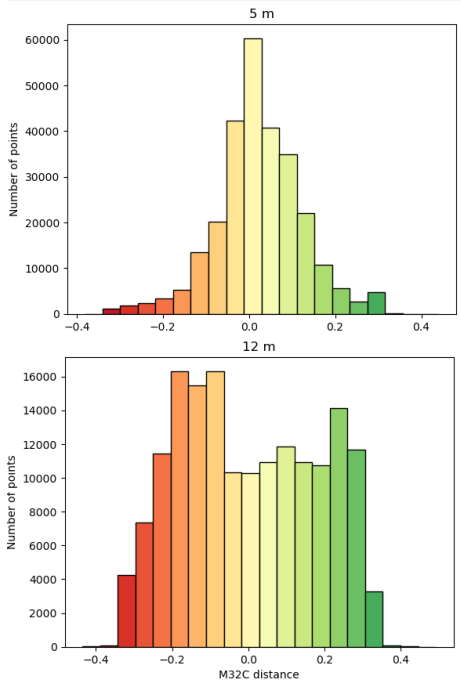

Figure 8. M3C2 distance between TLS and photogrammetric point clouds for A1 at 5 m (top) and 12 m (bottom).

The branch density is highly reflected in the distribution of points within the photogrammetric point clouds. Due to the field of view, all of the point clouds have a very high proportion of points on the tree trunk at shorter distances - most branches are not visible in the image. However, for the trees where the tree crown is not very dense, the points are more distributed across the branches the further the image is taken from the target. This is the case for both ash trees. Sycamore has a dense

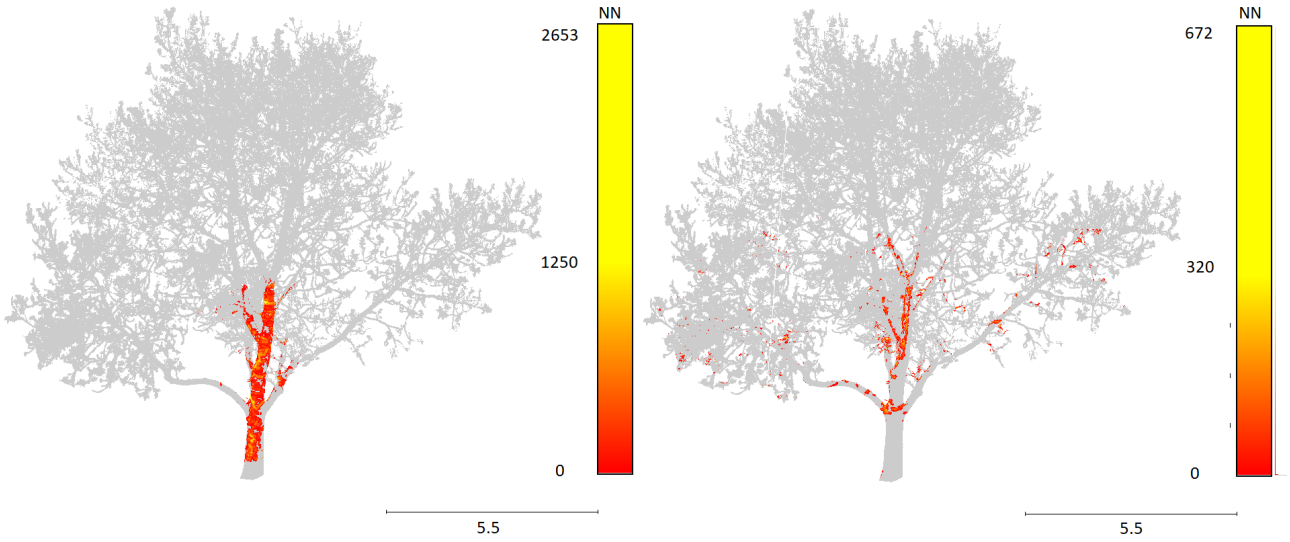

Figure 9. Nearest-neighbours number of points for Ash (A1) at the distance of 5 m (left) and 12 m (right). Grey points indicate areas not covered by the photogrammetric point cloud.

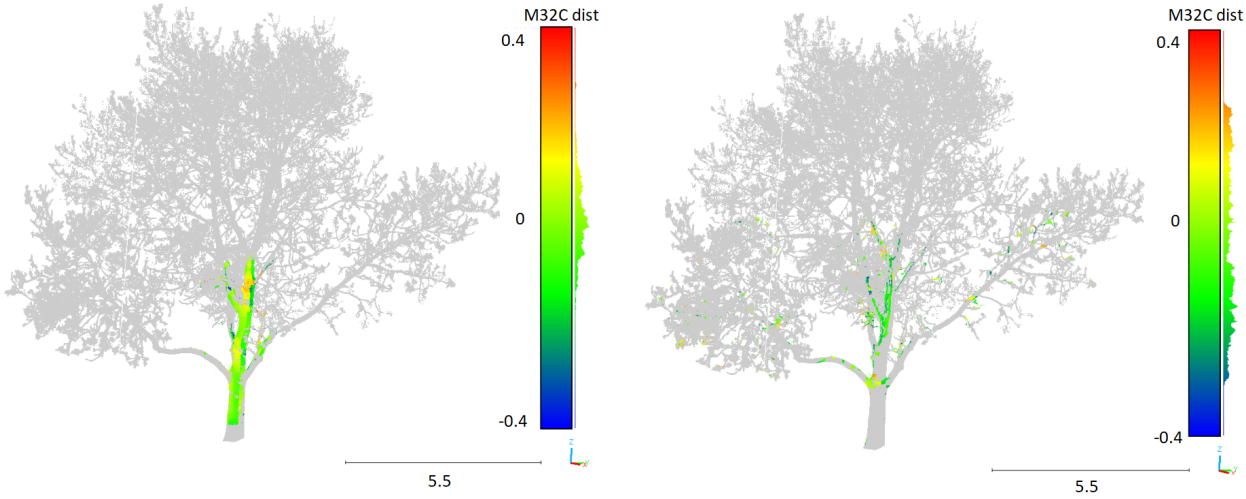

Figure 10. M3C2 distance for Ash (A1) at the distance of 5 m (left) and 12 m (right). Grey points indicate areas not covered by the photogrammetric point cloud.

crown that was more difficult to reconstruct, hence the points are still mostly focused on the trunk, regardless of the distance. A similar observation applies to lime, although here the issue is more related to the presence of foliage during the data capture rather than the density of branches within the crown (Figure 7). There is no strong pattern present in W1, but that may be due to the relatively small size of the point clouds, with very little coverage across the tree.

4.4 Point cloud distance (M3C2)

In order to examine the alignment and distribution of photogrammetric points in relation to laser scanning, we calculated the M3C2 distance between the point clouds. It was found that in most cases, across the species and distances, the photogrammetric and laser scanning point clouds are well aligned, with most points at M3C2 distance 0. An example of such distribution can be seen in Figure 8. The one exception is A1, where the M3C2 deviation is higher across the point cloud in both directions. When comparing the nearest-neighbour point distribution across the tree (Figure 9), it can be seen that at a distance of 5 metres, the points are highly concentrated on the tree trunk, and the surface is well reconstructed and aligned with the TLS. At a distance of 12 metres, the points are more distributed across the tree, particularly the prominent first-order branches, with the highest concentration of points in the areas where the branches meet the trunk. In terms of M3C2 distance (Figure 10), higher deviations can be seen in the branches and the further from the tree trunk, the higher the deviation. This may indicate the errors in depth resolution due to the increase in distance from the target.

5. DISCUSSION AND CONCLUSIONS

The low-cost photogrammetric system introduced in this study has the capability to provide a rough reconstruction of the tree architecture, however with significant limitations. With images taken at a close distance to the target tree, it is possible to reconstruct the tree trunk with high point density. In most cases,

the further the image from the tree, the more distributed the points across the crown, but also the resulting point cloud is significantly sparser. As from the perspective of stability assessment, we are mostly interested in the tree trunk and major branches, it is essential to find an optimal distance that provides a sufficient field of view, with points distributed across the relevant areas. A larger distance of the cameras from the tree may also introduce a depth error to the point cloud, which may be detrimental to sway monitoring, as the actual positions of the branches will have higher uncertainty, however, we are mostly interested in the relative position rather than absolute. Although the point clouds are sparse, skeletonization methods could potentially be applied to reconstruct the branching structure of the trees from the points. There are also limitations to the data acquisition, which have implications for the quality of the point clouds. The images were taken in late April and early May and some of the trees have already grown leaves. This issue has been most prominent in the case of lime and whitebeam. Additionally, as whitebeam has a very dense crown of very fine branches, it is most difficult to detect and match the keypoints. Future research should consider datasets from both leaf-on and leaf-off stages, as means of comparison - while it may be easy to retrieve the branching structure from a tree without foliage, it may not be possible for the same tree, but with the leaves present. Another major obstacle to the reconstruction of the trees was inconsistent light. The camera settings were set as constant values. This was supposed to ensure that both of the cameras provide consistent images at the same time. Automatics settings can sometimes lead to inconsistency between the images, as the change in setting can be triggered in one but not the other camera. These settings were not adjusted between the acquisitions at each distance, so changing weather and sun position affected the illumination. While in general, we found the reconstruction to be of higher quality in brighter images, more work is required to determine what settings of exposure and what amount of light is necessary to obtain the most optimal result. It also has to be noted that this is the most basic version of the system. Future iterations might explore the potential of a higher number of cameras installed on the same rail, which would allow for a larger overlap between the photos and higher quality of the point cloud, but also increase the cost of the system and could be detrimental to its portability and deployability. The use of fisheye lenses instead of pinhole cameras is another aspect worth exploring in the future, as fisheye lenses provide a larger field of view, potentially improving the capture and reconstruction of tree canopies at closer distances and smaller baselines. While NoIR cameras are used in this study, their spectral capabilities are not explored. Future work should take the spectral properties into consideration, as they can provide us with additional data in the form of e.g vegetation indices which may have implications for the tree health assessment.

6. ACKNOWLEDGEMENTS

This research was funded by the EPSRC Centre for Doctoral Training (CDT) in Geospatial Systems (ref EP/S023577/1).

REFERENCES

Agisoft, 2023. Agisoft Metashape Professional Edition.

CloudCompare, Z., 2020. CloudCompare: 3D point cloud and mesh processing software.

Cutugno, M., Robustelli, U., Pugliano, G., 2022. Structure-from-Motion 3D Reconstruction of the Historical Overpass Ponte della Cerra: A Comparison between MicMacreg; Open Source Software and Metashapereg;. *Drones*, 6(9). https://www.mdpi.com/2504-446X/6/9/242.

Doick, K. J., Peace, A., Hutchings, T. R., 2014. The role of one large greenspace in mitigating London's nocturnal urban heat island. *Science of The Total Environment*, 493, 662-671.

Jaalama, K., Kauhanen, H., Keitaanniemi, A., Rantanen, T., Virtanen, J. P., Julin, A., Vaaja, M., Ingman, M., Ahlavuo, M., Hyyppä, H., 2021. 3D Point Cloud Data in Conveying Information for Local Green Factor Assessment. *ISPRS International Journal of Geo-Information 2021, Vol. 10, Page 762*, 10, 762. https://www.mdpi.com/2220-9964/10/11/762/htm https://www.mdpi.com/2220-9964/10/11/762.

Jackson, T., Sethi, S., Dellwik, E., Angelou, N., Bunce, A., van Emmerik, T., Duperat, M., Ruel, J.-C., Wellpott, A., Van Bloem, S., Achim, A., Kane, B., Ciruzzi, D., Loheide II, S., James, K., Burcham, D., Moore, J., Schindler, D., Kolbe, S., Wiegmann, K., Rudnicki, M., Lieffers, V., Selker, J., Gougherty, A., Newson, T., Koeser, A., Miesbauer, J., Samelson, R., Wagner, J., Coomes, D., Gardiner, B., 2020. The motion of trees in the wind: a data synthesis. *Biogeosciences Discussions*, 1–21.

Ko, C. ., Lee, J. ., Kim, D. ., Kang, J., Buddenbaum, H., Ko, C., Lee, J., Kim, D., Kang, J., 2022. The Application of Terrestrial Light Detection and Ranging to Forest Resource Inventories for Timber Yield and Carbon Sink Estimation. *Forests 2022, Vol. 13, Page 2087*, 13, 2087. https://www.mdpi.com/1999-4907/13/12/2087/htm https://www.mdpi.com/1999-4907/13/12/2087.

Lague, D., Brodu, N., Leroux, J., 2013. Accurate 3D comparison of complex topography with terrestrial laser scanner: Application to the Rangitikei canyon (N-Z). *ISPRS Journal of Photogrammetry and Remote Sensing*, 82, 10-26.

Miller, J., Morgenroth, J., Gomez, C., 2015. 3D modelling of individual trees using a handheld camera: Accuracy of height, diameter and volume estimates. *Urban Forestry and Urban Greening*, 14, 932-940.

Mokroš, M., Koreň, A. M., Čerňava, J., Zápotocký, M., Tomaštík, J., 2017. First test of low-cost single-board computer based camera for close-range forest photogrammetry. *International Multidisciplinary Scientific GeoConference: SGEM; Sofia*, 17, 529-535. https://doi.org/10.5593/sgem2017H/33.

Nelson, M. F., Klein, R. W., Koeser, A. K., Landry, S. M., Kane, B., 2022. The Impact of Visual Defects and Neighboring Trees on Wind-Related Tree Failures. *Forests 2022, Vol. 13, Page 978*, 13, 978. https://www.mdpi.com/1999-4907/13/7/978/htm https://www.mdpi.com/1999-4907/13/7/978.

Raumonen, P., 2017. TreeQSM: Quantitative structure models of single trees from laser scanner data. *MATLAB-software TreeQSM User Guide v*, 2, 27.

Sousa-Silva, R., Duflos, M., Barona, C. O., Paquette, A., 2023. Keys to better planning and integrating urban tree planting initiatives. *Landscape and Urban Planning*, 231, 104649.

Turner-Skoff, J. B., Cavender, N., 2019. The benefits of trees for livable and sustainable communities. *Plants, People, Planet*, 1, 323-335. https://onlinelibrary.wiley.com/doi/full/10.1002/ppp3.39.

van Haaften, M. A., Meuwissen, M. P., Gardebroek, C., Kopinga, J., 2016. Trends in financial damage related to urban tree failure in the Netherlands. *Urban Forestry and Urban Greening*, 15, 15–21.

Willis, K. J., Petrokofsky, G., 2017. The natural capital of city trees. *Science*, 356, 374-376. https://www.science.org/doi/10.1126/science.aam9724.